九州大学学術情報リポジトリ
Kyushu University Institutional Repository

Exploring Metal Cluster Catalysts Using Swarm Intelligence: Start with Hydrogen Adsorption

Tsuji, Yuta
Institute for Materials Chemistry and Engineering, Kyushu University

Yoshioka, Yuta
Institute for Materials Chemistry and Engineering, Kyushu University

Hori, Mikiya
Institute for Materials Chemistry and Engineering, Kyushu University

Yoshizawa, Kazunari
Institute for Materials Chemistry and Engineering, Kyushu University

https://hdl.handle.net/2324/7437556

出版情報：Topics in Catalysis. 65 (1-4), pp.215-227, 2021-10-01. Springer
バージョン：
権利関係：This version of the article has been accepted for publication, after peer review (when applicable) and is subject to Springer Nature’s AM terms of use, but is not the Version of Record and does not reflect post-acceptance improvements, or any corrections. The Version of Record is available online at: http://dx.doi.org/10.1007/s11244-021-01512-2

KYUSHU UNIVERSITY

Exploring Metal Cluster Catalysts Using Swarm Intelligence: Start with Hydrogen Adsorption

Yuta Tsuji,* Yuta Yoshioka, Mikiya Hori, and Kazunari Yoshizawa*

Institute for Materials Chemistry and Engineering and IRCCS, Kyushu University, Nishi-ku, Fukuoka 819-0395, Japan

Author Information

Corresponding Author

*E-mail: yuta@ms.ifoc.kyushu-u.ac.jp, kazunari@ms.ifoc.kyushu-u.ac.jp.

ORCID

Yuta Tsuji: 0000-0003-4224-4532

Kazunari Yoshizawa: 0000-0002-6279-9722

Abstract:

The catalytic function of metal nanoclusters has attracted much attention because of their specific activity and selectivity. The structures of metal clusters are very diverse, especially when adsorbates are adsorbed on them. This is an obstacle when approaching metal nanocluster catalysts with computational chemistry. In this manuscript, a prescription for this problem is presented. With metal nanoclusters catalyzing reactions involving hydrogen in mind, a comprehensive, systematic, and efficient search for stable structures of metal nanoclusters with an adsorbed hydrogen atom is presented. This can be achieved through a good use of a supercomputer while using the particle swarm optimization algorithm and density functional theory together. In this attempt, three metallic elements, Fe, Ni, and Cu, are selected. When clustered, what kind of structure these elements form and how their affinity for hydrogen changes are detailed. Eventually, a path is presented to explore clusters that are actually useful as catalysts, using surface calculations as a reference.

Keywords: Metal clusters, Swarm intelligence, Particle swarm optimization, Hydrogen adsorption, Density functional theory

1 Introduction

There are a great variety of processes involving hydrogen in heterogeneous catalysis. Surface processes involving hydrogen include hydrogen adsorption/desorption, H-H activation, and hydrogen spillover. Hydrogen-related reactions include hydrogen evolution, ammonia synthesis, and carbon dioxide reduction. These processes often involve catalyst-hydrogen reactions. Appropriate evaluation of catalyst-hydrogen interactions is expected to make it possible to select a suitable catalyst for the reaction. Transition metal surfaces are often used to study catalysts for hydrogen adsorption reactions because they are frequently used to catalyze industrially relevant chemical reactions [1].

There is a wide range of transition metals whose interactions with hydrogen have been systematically investigated. Iron is widely known for its industrial use as a heterogeneous catalyst. For example, the Haber-Bosch process [2] and the Fischer-Tropsch synthesis [3, 4, 5] are two of the most important large-scale industrial processes where hydrogen is used as the main reactant. The energy and structure of hydrogen adsorption on iron surfaces have been clarified by using periodic density functional theory (DFT) calculations [6]. Even if the system is huge and/or magnetic, it can be treated appropriately.

Nickel is as important a catalyst as iron. Paul Sabatie discovered that using a small amount of nickel as a catalyst, hydrogen can be added to unsaturated hydrocarbons such as alkenes. For his work, he was awarded the Nobel Prize in Chemistry in 1912 [7]. The Sabatier

reaction, in which hydrogen and carbon dioxide are placed under high temperature and pressure to produce methane and water using nickel as a catalyst, is also known [8]. Conversely, nickel can be used in the production of syngas, comprising hydrogen and carbon monoxide, in steam reforming of hydrocarbons [9]. These catalytic reactions cannot be described without mentioning the interaction of hydrogen with the nickel surface. The adsorption and dissociation of hydrogen on the nickel surface has been thoroughly investigated [10, 11, 12].

Copper catalysts can catalyze a limited number of reactions, such as hydrogenation, dehydrogenation, and oxidation, their activity not high. However, copper-based catalysts are cost-effective for many chemical processes [13]. Copper catalysts are known to be used for selective hydrogenation of nitrobenzene to aniline [14]. They are also known to exhibit high selectivity in dehydrogenation of alcohols [15, 16]. Here, again, hydrogen plays an important role. The dissociation behavior of molecular hydrogen on Cu surfaces has been systematized in theoretical studies [17, 18].

Metal species of different sizes (monatomic, nanoclusters, and nanoparticles) exhibit different catalytic activities in a variety of heterogeneous catalytic reactions [19]. Sub-nanometer-sized metal clusters are known to have properties that are very different from those of nanoparticles, and their catalytic functions have attracted much attention because of their specific activity and selectivity [20, 21, 22]. Many factors such as cluster size, shape, chemical composition, and metal-support interaction have been shown in the literature to have a

significant effect on the catalytic properties [19, 23].

Recently, transition metal nanoclusters that catalyze reactions involving hydrogen have also been attracting attention. Hosono and co-workers investigated in detail the kinetics of ammonia synthesis using ruthenium clusters supported on an electride and found that, unlike the Haber-Bosch process, the formation of NH_n species is a rate-limiting step [24]. Recently, by reducing the size of copper particles to a very small size, Tada and co-workers have developed a catalyst that converts carbon dioxide into methanol with high efficiency [25]. The effectiveness of metal nanoclusters has been experimentally confirmed in various other catalytic reactions involving hydrogen; for example, hydrogenation of arenes using rhodium nanoclusters stabilized in ionic liquids [26] and dehydrogenation of aliphatic secondary alcohols and formic acid using Pt nanoclusters supported on metal oxides [27] and phosphorous-alloyed Pd nanoclusters [28], respectively. We are aware that there are too many experimental studies on nanocluster catalysis to cite here, even if we restrict ourselves to reactions involving hydrogen. However, this manuscript is not intended to be a review of them, so we move on.

Theoretical approaches to metal nanocluster catalysis involving hydrogen are also very useful tools. In the literature, one can find theoretical studies on the C-H bond activation of methane on Ni and Pt nanoclusters supported on CeO_2 [29, 30], and those in which the authors found that copper nanoclusters can be used as catalysts for the hydrogenation of acetylene and

ethylene [31]. It may go without saying that insights into the interaction of metal nanoclusters with hydrogen atoms will play an important role in these reactions.

When it comes to bulk metal surfaces, it has been reported that hydrogen affinity to metal surfaces is a good descriptor for the reactivity of the catalyst to methane [32, 33]. It would also be worth noting that the strength of the interaction between hydride surfaces and hydrogen is the key to revealing the catalytic activity of hydride catalysts for ammonia synthesis [34, 35, 36]. We have not yet found any such examples as far as metal clusters go. However, we are not claiming that humanity's knowledge of the adsorption behavior of hydrogen on metal nanoclusters is inadequate. First-principles calculations have gone a long way toward reinforcing it.

With DFT calculations, it has been revealed that the adsorption energy of hydrogen to metal nanoclusters is highly dependent on the composition of the cluster and that the details of the reaction thereon can be elucidated from the changes in the local charges of hydrogen and the constituent atoms of the clusters [37]. DFT calculations also identified that copper and gold nanoclusters have small fluctuating adsorption energies with respect to the increase in the number of adsorbed hydrogen atoms [38]. By combining theoretical and experimental methods, it is possible to clarify the details of the bonding between metal clusters and hydrogen [39].

In most of the previous theoretical studies, the target is limited to metallic nanoclusters of a specific element or number of constituent atoms. We are well aware of the fact that

calculations cannot be performed without narrowing down the target. However, a systematic comparison of the adsorption behavior and interaction of hydrogen atoms across multiple metal species and multiple numbers of constituent atoms should be made. There are many factors that get in the way of this, such as limited computational resources. We have worked hard to get past it, and other theorists [40, 41] are working on it, too.

Herein, we would like to introduce our recent work in pioneering a novel method of catalyst discovery based on the efficient optimization of hydrogen adsorption structures on metal clusters using swarm intelligence [42]. More specifically, this manuscript describes the results of the search for stably adsorbed structures of a hydrogen atom on each of Fe, Ni, and Cu nanoclusters with the number of atoms up to 10 as well as the theoretical analysis of the interaction of the hydrogen atom to the clusters. Eventually, clues to catalyst design will be obtained by comparing the adsorption of hydrogen on the clusters with that on a typical heterogeneous catalyst surface.

2 Theoretical Methods

The adsorption sites of hydrogen atoms on close-packed metal surfaces are only on-top, bridge, and hollow [43]. However, since the structure of metal nanoclusters is very diverse and many isomers exist, it would be necessary to consider more adsorption sites and adsorption conformations than on metal surfaces [44, 45, 46, 47]. Therefore, manually analyzing the

adsorption site of even a single hydrogen atom on metal nanoclusters one by one would require a great deal of effort, computational cost, and time.

In order to efficiently search for the most stable hydrogen-adsorbed structure of metal nanoclusters, we used the Crystal structure AnaLYsis by Particle Swarm Optimization (CALYPSO) program [48, 49, 50]. Particle Swarm Optimization (PSO), a type of swarm intelligence, is a population-based optimization method first proposed by Kennedy and Eberhart [51, 52]. PSO, a stochastic global optimization method, was inspired by the dynamics of bird flocking and can be viewed as a distributed behavioral algorithm for multidimensional space exploration [49]. In the process of PSO, each individual flies through hyperspace under the influence of the individual in the local optimal position or the individual with the best fit in the entire population so far. In addition, individuals can learn from past experiences and adjust their flight speed and direction. In this way, all the individuals that make up the swarm can quickly converge to the global optimal position.

It should be noted that PSO is not the only way to search for stable cluster structures. For example, one could use genetic algorithms (GA) or Bayesian optimization (BO). PSO and GA can be classified as evolutionary algorithms [53]. This type of algorithm puts emphasis on structure search through generational change. On the other hand, BO is a selection type algorithm that can efficiently select candidates from a large number of structures by machine learning [53]. A comparison of PSO and GA in terms of cluster structure search has already

been discussed in the literature [54, 55]; the main difference would be that GA has a selection process characterized by the survival of the fittest, while PSO does not include such a process. It has been reported that PSO requires a relatively small population size and shows fast convergence compared with GA [55]. As for BO, it is not in conflict with the evolutionary algorithms. Once a large number of structures are generated by the evolutionary algorithm, the candidate structures can be efficiently selected by using BO [53]. As such, it may be possible to find the global minimal structure in much fewer trials. We are not able to use such a method at present, but in this way, it may be possible to search for the most stable cluster structure in the future.

In considering conducting a PSO calculation with CALYPSO, it is important to note that CALYPSO itself does not solve the Schrödinger equation, so one needs a DFT-equipped sidekick to diagonalize the Hamiltonian for clusters and optimize their structures locally. For this purpose, we used the Vienna ab initio simulation package (VASP) [56, 57, 58, 59]. The reader may question our choice, for VASP is a plane-wave based DFT program suitable for periodic systems. However, the cluster can be calculated by using a unit cell with a vacuum layer of about 15 Å thick introduced in the a, b, and c-axis directions around it, as shown in Fig. 1. We have performed benchmark calculations in our previous studies and have already confirmed that the cluster structures optimized with this method agree well with those optimized with software for molecular calculations such as Gaussian [60, 61]. The calculation

of metal clusters using CALYPSO is not something that we have devised. It is a general method that has been adopted by many groups [62, 63, 64]. The calculation of metal clusters using VASP is not uncommon, either [65, 66, 67].

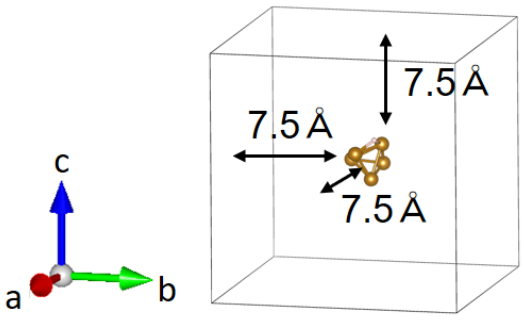

Fig. 1 Example of a periodic boundary cell for computing metal clusters using VASP.

The novelty of our research is that we seek the most stable adsorption structure of a substrate on a metal cluster by optimizing the cluster together with the substrate with catalyst search in mind. Such a process can be automated, providing a comprehensive set of data that may be critical for catalyst development. We are cultivating the soil for catalyst informatics [68, 69, 70] to flourish in the future.

With the aid of CALYPSO and VASP, the most stable structure among nanoclusters consisting of one H and n M (M = Fe, Ni, or Cu; n = 1–10) atoms were explored. For comparison, the stable geometry for each M_n structure was determined by exploring the most stable structure in a system with only n M atoms in the unit cell. The reasons for our selection of these metals

would be clear from the second through fourth paragraph of the introductory part of this manuscript.

The generalized gradient approximation of Perdew, Burke, and Ernzerhof (GGA-PBE) [71] was used as the density functional. Software for molecular calculations, such as Gaussian, can perform fast calculations using a hybrid functional and provide highly accurate results, but it is not realistic to use it in VASP to perform structure searches. Therefore, care should be taken when comparing the energies presented in this study with those calculated using other functionals. In the Electronic Supplementary Information (ESI), we have discussed the difference in energy due to differences in programs and calculation methods. The structural optimization conditions were set so that the cutoff energy was 400 eV and the k-point was sampled only at the Γ point within the Brillouin zone. The projector augmented wave method [72, 73] was used for the pseudopotential. The convergence condition for the self-consistent field (SCF) calculations was set to 1.0×10^{-4} eV and that for the structural optimization to 1.0×10^{-3} eV. Grimme's D2 method [74] was used as the dispersion correction. The spin polarization was taken into account in all the calculations. We have thoroughly verified the validity of the VASP spin polarization calculation in our previous study [60], so we can use it with confidence in the present study. Information of the magnetic moments of the metal clusters optimized is available in the ESI.

When generating a new group (next generation) in the PSO process, the number of

structures per generation (population) was set to 20, 80% of which were generated using the PSO algorithm, and the remaining 20% were generated randomly. The PSO calculation using CALYPSO was considered to have converged if there was no update of the most stable structure for more than 10 generations.

Due to the randomness involved in the search, one might be concerned that each time the calculation is performed, a different stable structure will be obtained. However, as seen in the ESI, two calculations done independently present the same structure. On top of that, doing the same thing with different elements did not change the conclusion. It would be safe to say that the cluster structures explored with our method are most likely global minimum structures.

In order to optimize a very large number of structures in the structure search using CALYPSO, the structural optimization in the PSO process was performed under relatively loose conditions as described above. In order to calculate and better understand the detailed geometrical and electronic structures of the most stable structures obtained, the structural optimization of these structures was performed again under more precise conditions: the convergence condition of the SCF was changed to 1.0×10^{-5} eV, the convergence condition of the structural optimization to 1.0×10^{-4} eV, and the cutoff energy to 500 eV. The other calculation conditions were the same as those described above. The structure drawing program of VESTA [75] was used to visualize optimized cluster structures throughout this manuscript.

3 Results and Discussion

3.1 Stable Hydrogen Adsorption Structures on Nanoclusters

The most stable structures of the metal nanoclusters alone and those of the system consisting of metal nanoclusters and one hydrogen atom, obtained as a result of the PSO structure search, are shown in the upper and lower rows in each panel of Figs 2 and 3, respectively. In interpreting these figures, one may assume that the addition of one hydrogen atom to the metal cluster structures shown in the upper row produces the structures shown in the lower row. However, it should be noted that the most stable structure was determined by PSO before and after hydrogenation separately. We would like to emphasize that CALYPSO did not refer to the structures of the clusters without hydrogen in the structure search of the metal clusters with hydrogen. They are the results of completely independent calculations. Since catalytic reactions usually occur after the catalyst itself has been synthesized, it seems more natural to use PSO to explore which sites are most stable for H adsorption on the most stable M_n clusters obtained using PSO beforehand. However, we are not able to perform such a method at present. Nevertheless, we have calculated an energy diagram connecting the structure obtained from a posteriori addition of H to the most stable metal cluster explored with PSO and the most stable cluster structure explored with H included in advance. The energy barrier associated with the structural change from the former to the latter are discussed in the ESI. Interestingly, the barrier was found not to be high.

Another caveat in understanding the structures is that these are the most stable structures in the ground state at $T \to 0$ K; as shown in the ESI, there are many isomers in a narrow energy range, so the most stable structure may change at high temperatures due to entropy effects. The entropy effect in such small size clusters has been estimated in our previous study [60].

First, let us look at the system with up to five metal atoms. At a glance, it can be seen that the effect of hydrogen addition on the structures of the metal clusters is extremely small. The addition of one hydrogen atom to the system does not change the structure of the metal cluster itself at all. One can notice that Cu clusters tend to have a planar conformation regardless of the presence or absence of hydrogen. In complex chemistry, it is well known that Cu complexes form a planar four-coordinate structure [76, 77, 78]. This property may be reflected in the Cu cluster structures. We are currently in the process of developing a more general and comprehensive framework for understanding the geometrical features of metal clusters. When the time comes, we may be able to show it elsewhere.

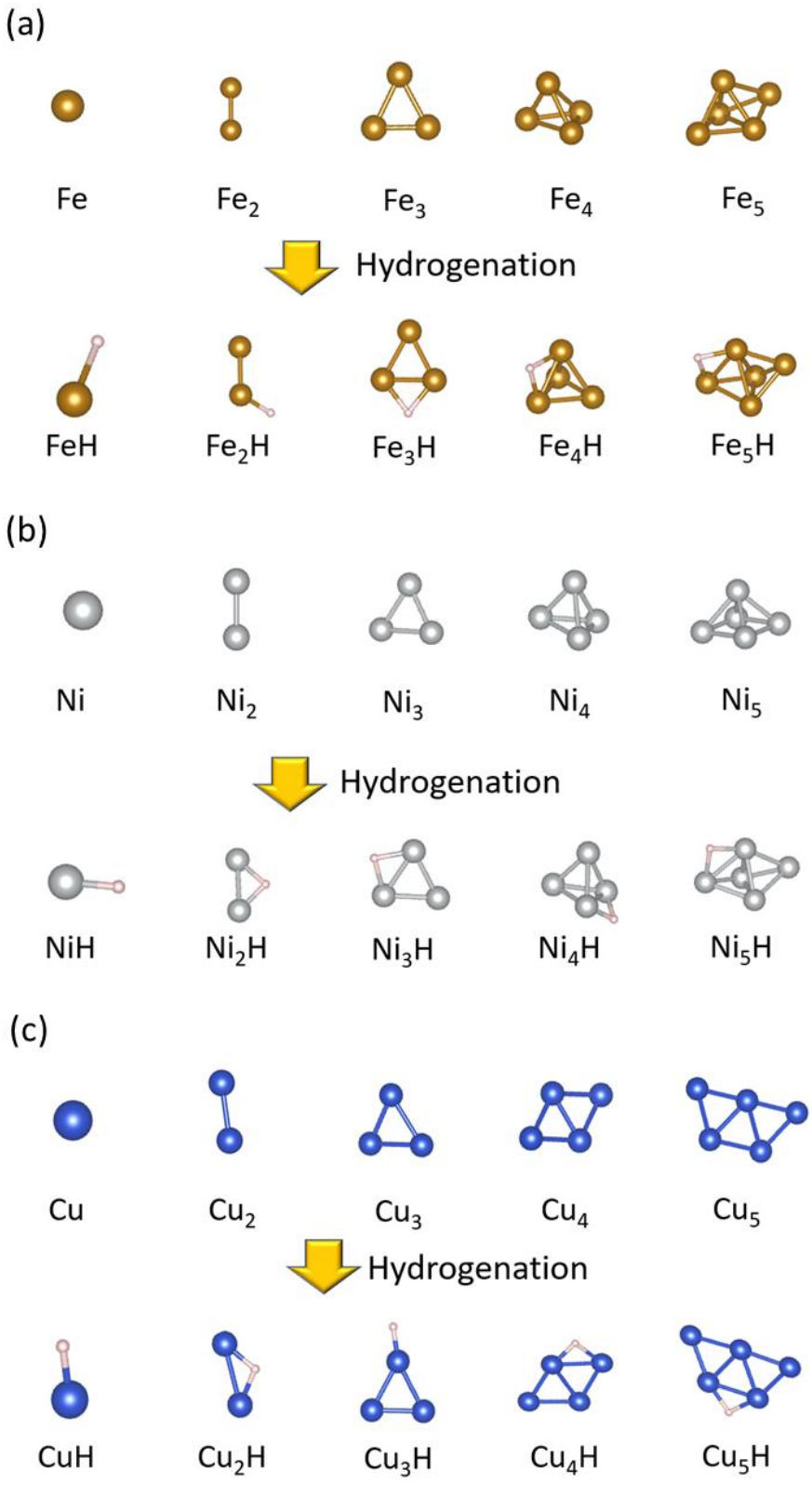

Fig. 2 The most stable cluster structures of M_n and M_nH (M = Fe (a), Ni (b), Cu (c); n = 1-5) obtained from our structural search. Fe–Fe, Ni–Ni, and Cu–Cu bonds are shown only when the bond length is 3.0 Å or less. Fe–H, Ni–H, and Cu–H bonds are shown only when the bond length is 2.0 Å or less.

What happens when the number of metal atoms is further increased? Let us look at the cases where n = 6-10. As for the Cu clusters, the change in the cluster structure is more pronounced than in the Fe and Ni ones. As n increases to 9 or 10, structural changes due to adsorption of a hydrogen atom can also be observed in the Ni clusters. In the case of the Fe clusters, no significant deformation of the structure due to hydrogen adsorption was observed. This suggests that the Cu clusters are soft compared to the Ni and Fe ones. One may link this observation to the variation of the cohesive energy of transition metals with the filling of the d band, which is well known in solid state physics [79].

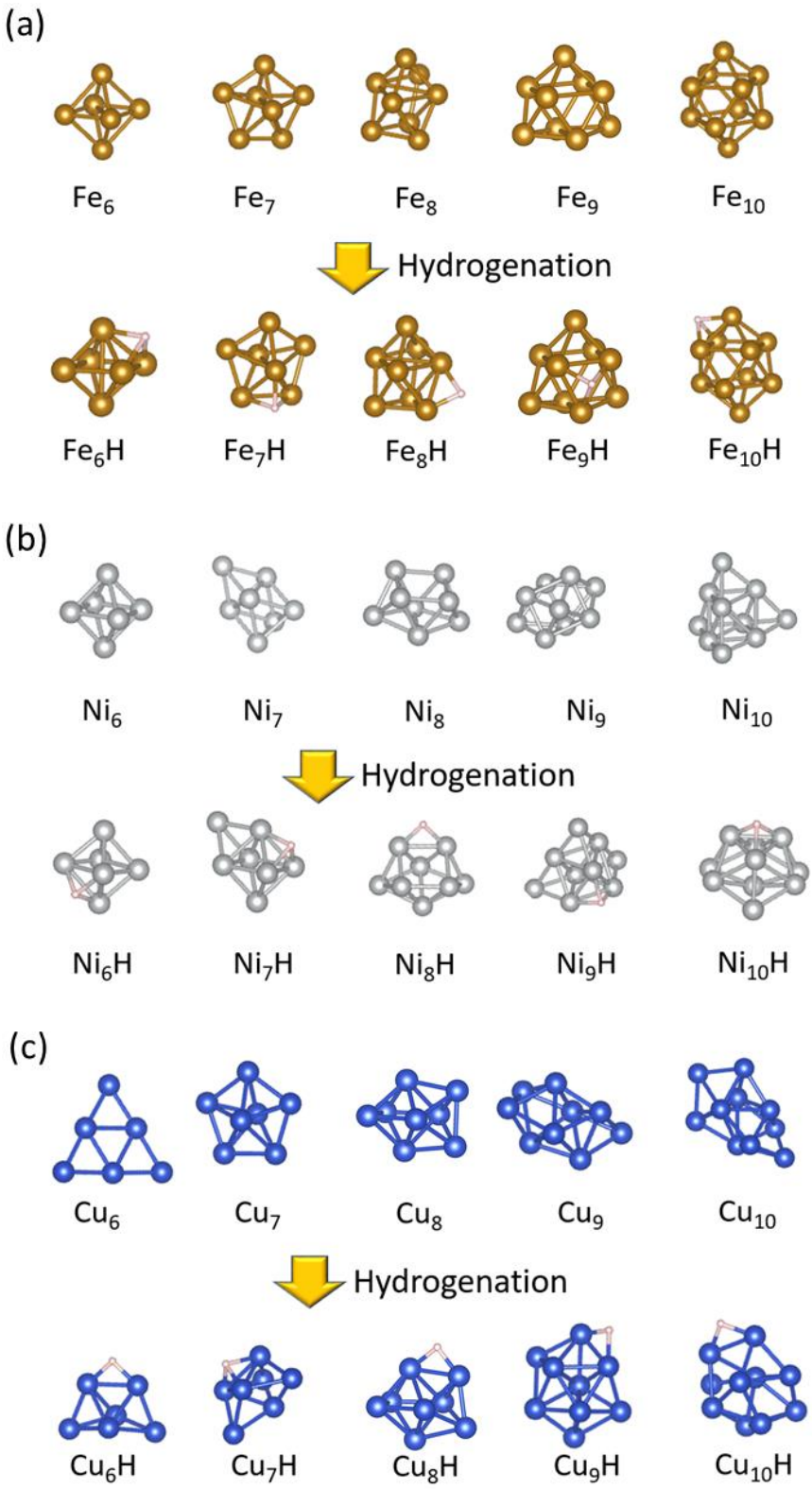

Fig. 3 The most stable cluster structures of M_n and M_nH (M = Fe (a), Ni (b), Cu (c); n = 6-10) obtained from our structural search. Fe–Fe, Ni–Ni, and Cu–Cu bonds are shown only when the bond length is 3.0 Å or less. Fe–H, Ni–H, and Cu–H bonds are shown only when the bond length is 2.0 Å or less.

Now, let us look at the structure a little more from another perspective. Fig. 4 shows how the radial distribution function (RDF), *g*, for metal-metal distances, *r*, in the clusters changes before and after the adsorption of the hydrogen atom. For each metal, one can identify a well-developed first coordination sphere. For Fe, its peak is characteristically divided into two.

Since the position of the peak does not change before and after the adsorption of the hydrogen atom, it can be said that the effect of the hydrogen adsorption on the metal-metal bond length is very small. The position of the peak is at r = 2.3 Å for Ni, and the larger peak is there for Fe as well. That of Cu is at r = 2.4 Å, which again may reflect the weaker nature of the Cu-Cu bond.

It is also worth noting the change in peak height. A sharp, high peak means that there is a high probability of finding an atom at a particular distance. As the structural order is lost, it goes down. Comparing the RDF peaks for crystal, amorphous, and solution, the differences are quite striking [80]. It is natural that the peak height becomes lower when the hydrogen atom is adsorbed. The degree to which the peak height is lowered may be used to quantify the degree of structural deformation associated with hydrogen adsorption. The decrease in the peak height for Cu is most pronounced, consistent well with the structural deformation in the Cu clusters [81].

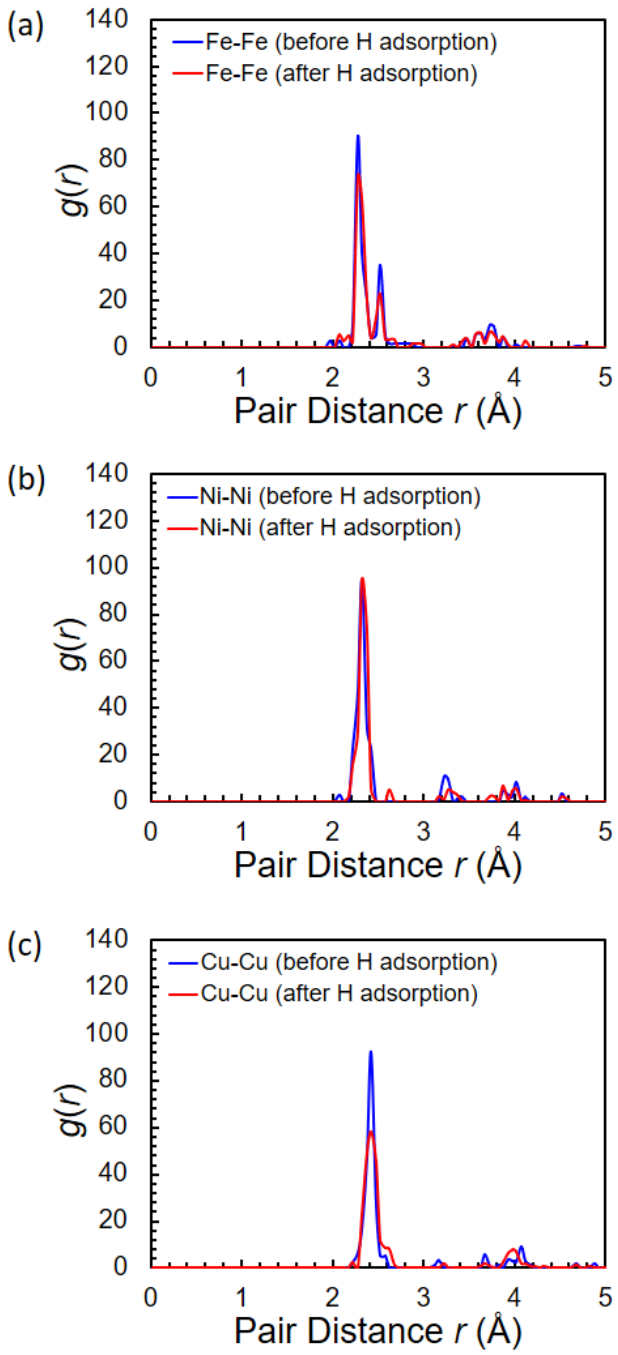

Fig. 4 Radial distribution function (RDF), *g*, for the metal-to-metal distance, *r*, in the Fe (a), Ni (b), and Cu (c) clusters before (blue) and after (red) hydrogen adsorption. For each metal species, the RDF plot was generated by taking into account all the structures shown in Figs 2 and 3.

We cannot close this section without mentioning the adsorption sites of the H atom. Let us go back to Figs 2 and 3. In most cases of Cu, Ni, and Fe, when n = 1-5, the H atom tends

to be adsorbed at the bridge site. For the cases where n = 6-10, Ni and Fe tend to adsorb H at the three-fold hollow site, while Cu still tends to adsorb H mainly at the bridge site. The adsorption of the H atom to the bridge site is commonly observed in the Cu, Ni, and Fe clusters with n = 8. A general conclusion to be drawn from what is presented here may be that hydrogen has very little probability of being adsorbed at the on-top site on metal clusters. H adsorption to the on-top site seems to occur only rarely when the number of metal atoms in the cluster is very small.

3.2 Strength of the Binding of H to Metal Nanoclusters

Let us evaluate the strength of the affinity of each metal cluster for H. This is a physical quantity that will be important in predicting the catalytic activity of the clusters. It is known that the higher the hydrogen affinity of a catalyst surface, the more reactive the site for activating C-H bonds of alkanes by direct hydrogen-abstraction [82]. Metal clusters with a very high affinity for hydrogen might also be excellent catalysts not only for dehydrogenation but also for H-H activation. However, too strong the affinity of catalyst for hydrogen is not necessarily a good thing.

Here is an example: when Ru, a typical catalyst for ammonia synthesis [83], is injected with electrons from a promoter, its affinity for hydrogen increases and the hydrogen atoms supplied during the reaction process cover the Ru surface, making it difficult for the reaction to

proceed [84, 85]. This is one of the serious problems in catalytic chemistry, called hydrogen poisoning. After all, it would be desirable for the catalyst to have a moderate affinity for hydrogen.

Now, let us see how strong the interaction between the metal clusters and hydrogen is in our optimized metal clusters with one hydrogen atom adsorbed, which are denoted as M_nH below. In order to calculate the binding energy between hydrogen and the clusters, we performed a single-point calculation for the structure of the clusters with the H atom removed. Such a structure is denoted as M'_n in the following. Here, the binding energy ΔE_b is defined by the following equation:

$$\Delta E_b = E(M_nH) - E(H) - E(M'_n), \quad (1)$$

where $E(M_nH)$, $E(H)$, and $E(M'_n)$ represent the energies of M_nH, H, and M'_n, respectively.

The ΔE_b values plotted against the number of metal atoms constituting the metal clusters for each metal species are shown in Fig. 5. In a report on the heat of adsorption of hydrogen on polycrystalline transition metal surfaces, it was suggested that the order of the strength of adsorption is approximately Ni > Fe > Cu [86], so a similar result was expected for metal nanoclusters. But things are not so simple. Only the n = 2 cluster follows this order of adsorption strength.

What we observe here is a pleasing result, suggesting that the nanoclustering of metals significantly changes the strength of the interaction between metals and hydrogen, which is not

seen on solid surfaces. Looking at the entire graph, the binding energy of the Cu and Fe clusters to H seems to vary greatly depending on the number of metal atoms, while the effect of the change in the number of metal atoms is relatively small for the Ni. It would be very interesting to note that the n = 5 through n = 7 clusters show the exact opposite trend to what is for the solid surface. With regard to nanoclusters, it can be said that the strength of the affinity for hydrogen and the way it changes as a function of the cluster size are not necessarily determined by the metal species per se.

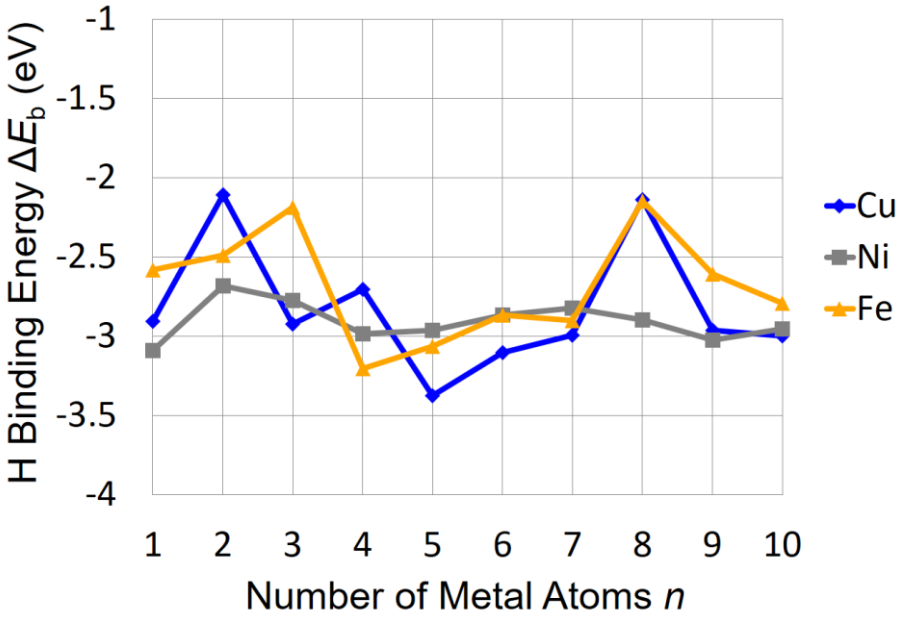

Fig. 5 H binding energy calculated for the metal clusters with one hydrogen atom adsorbed is plotted against the number of metal atoms in the cluster for each metal species.

In the calculations using eq. 1, the binding energy was evaluated by freezing the structure of the metal nanoclusters upon the elimination of H. Now, what about the energy of

what we call adsorption energy? Here, we define the adsorption energy ΔE_{ads} of the H atom to the metal nanoclusters as follows:

$$\Delta E_{\mathrm{ads}} = E(\mathrm{M_nH}) - E(\mathrm{H}) - E(\mathrm{M_n}), \quad (2)$$

where M_n denotes the global minimum structure of the nanocluster of the metal species M consisting of n atoms, obtained from the optimization using VASP and CALYPSO. It does not mean that we simply removed H from the structures shown in Figs 2 and 3 and optimized the clusters again with VASP, but that we referred to the most stable cluster structures without hydrogen also shown in Figs 2 and 3.

In that the structures of the metal clusters here are completely relaxed and no artificial fixation has intervened, we call the energy calculated from eq. 2 the adsorption energy. Care should be taken in comparing our results with those in the literature, since the energy reference there may be the H_2 molecule rather than the H atom.

The ΔE_{ads} values plotted against the number of metal atoms constituting the metal clusters for each metal species are shown in Fig. 6. Broadly speaking, there is no significant difference in the trends between Figs 5 and 6. However, it is worth pointing out some of minor differences. Only the clusters with n = 5 show a trend opposite to the order of strength of adsorption on the polycrystalline surfaces. As for Cu and Fe, the variation of the adsorption energy is slightly larger than that of the binding energy. On the other hand, the effect of the number of metal atoms on the adsorption energy of H to the Ni nanoclusters is still small.

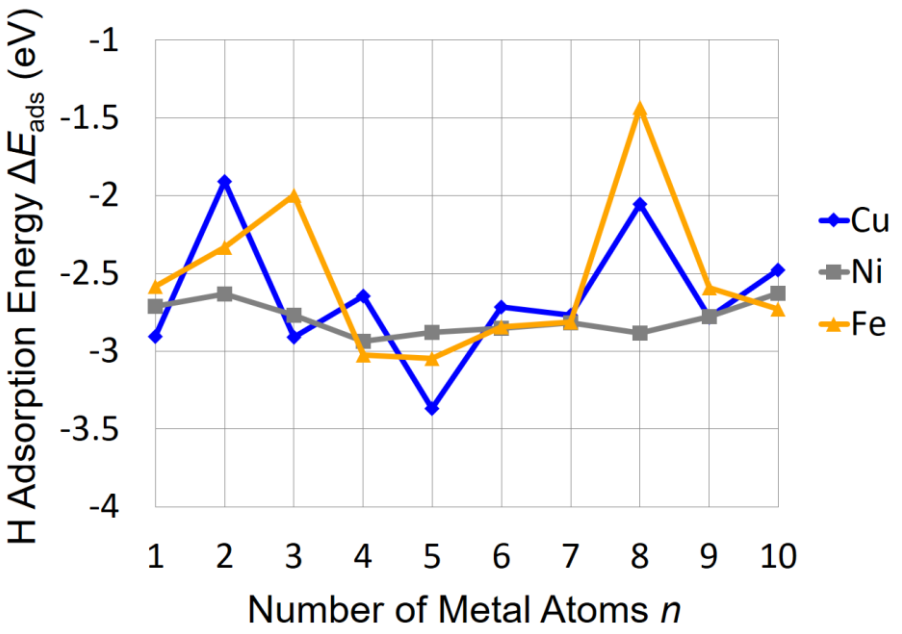

Fig. 6 H adsorption energy calculated for the metal clusters with one hydrogen atom adsorbed is plotted against the number of metal atoms in the cluster for each metal species.

For each metal species, we generated RDF plots for the metal-hydrogen distance, taking into account all the cluster structures where H is adsorbed, as shown in Fig. 7. What can we say about the interaction between hydrogen and metal from this figure? The first coordination sphere of the metal atoms around the hydrogen is found to be in the range of 1.4 to 2.0 Å. The center of the peak for Cu-H is located at a shorter distance than that for Fe-H. The graph of ΔE_b (Fig. 5) shows that the binding of the H atom is often stronger on the Cu cluster than on the Fe cluster of the same number of atoms. This observation may correspond to the difference in the peak positions. The narrower and more intense RDF peak of Ni-H seems to correspond well with the smaller variation of the binding energy of the H atom on the Ni clusters.

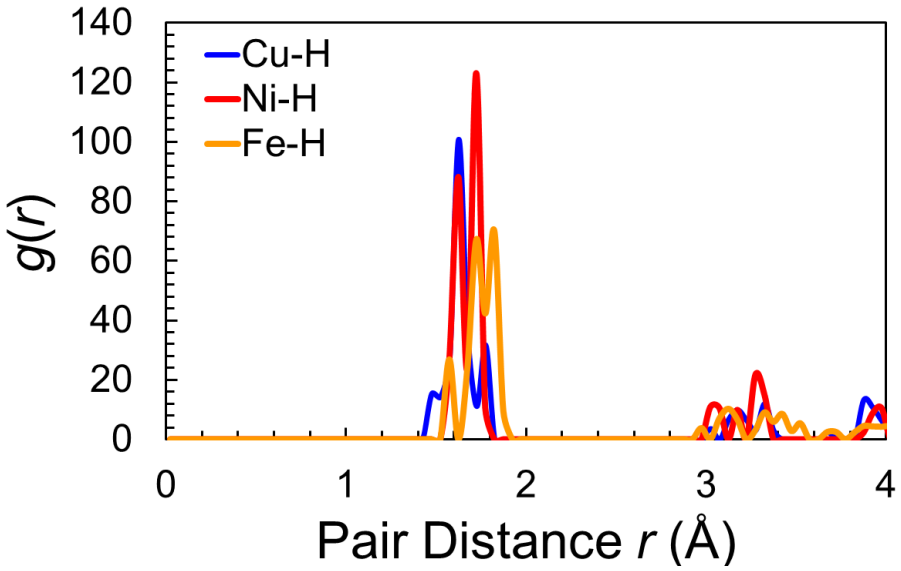

Fig. 7 RDF plots for the metal-to-hydrogen distance, *r*, generated by taking into account all the structures with the H atom shown in Figs 2 and 3.

3.3 Distortion of Metal Cluster Structures

The difference between the binding energy (Fig. 5) and the adsorption energy (Fig. 6) may be attributed to the destabilization due to the structural change of the metal nanoclusters as a result of H adsorption. By taking the difference between the binding and adsorption energies, one can quantify the destabilization energy. Therefore, we define the difference ΔE_{d} as follows:

$$\Delta E_{\mathrm{d}} = \Delta E_{\mathrm{ads}} - \Delta E_{\mathrm{b}} = E(\mathrm{M}_{\mathrm{n}}') - E(\mathrm{M}_{\mathrm{n}}). \qquad (3)$$

One may view ΔE_{d} as the energy associated with the distortion of the cluster structure, so it may deserve to be called the distortion energy. The perceptive reader may have already noticed our careful wording. The reason for this will soon become apparent.

The graph of ΔE_{d} plotted against the number of metal atoms for each metal species is

shown in Fig. 8. Figs 2 and 3 visually show the structural change of the nanoclusters upon H adsorption. From those figures, one can see that the structure of some nanoclusters changes significantly before and after hydrogen adsorption. Such nanoclusters appear to satisfy the condition of $\Delta E_d > 0.2$ eV. Conversely, it can be generally said that the smaller the value of ΔE_d, the smaller the structural change.

It should be noted, however, that the threshold number of 0.2 eV is just a good number as a delimiter and does not mean anything more than that. For example, ΔE_d for Cu_2 is slightly above 0.2 eV, but we cannot perceive any significant structural change in Fig. 2. Actually, the metal-metal bond length has changed by 0.3 Å, which is larger than that in Fe_2 and Ni_2 [87]. On the other hand, ΔE_d for Cu_9 is slightly below 0.2 eV, but we can recognize a relatively large structural change in Fig. 3.

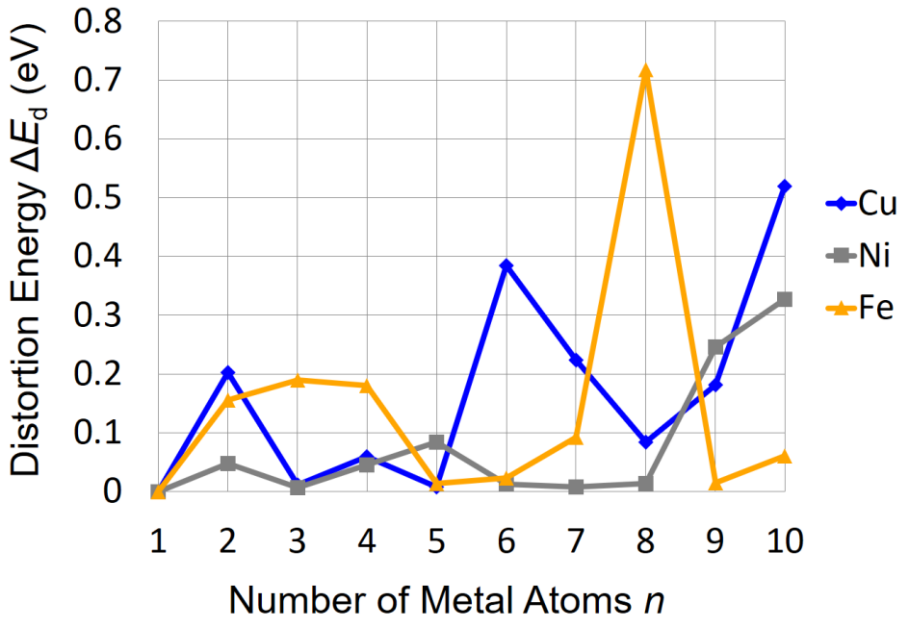

Fig. 8 Distortion energy of the metal clusters upon H adsorption is plotted against the number of metal atoms in the cluster for each metal species.

Since Fe_8 shows the largest ΔE_d value, one might expect that it would have undergone a significant structural change. However, Fig. 9 shows that this is not the case. We are still unable to determine the origin of the large ΔE_d value for Fe_8. At least, we have confirmed that magnetism is not the cause [88]. Therefore, here, we just report what we observed, leaving detailed analysis to future studies. On the other hand, the large ΔE_d value calculated for Cu_6 can be well understood. Before the adsorption of H, the Cu_6 cluster has a two-dimensional geometry, whereas after the H adsorption, it is stabilized in a three-dimensional geometry. The ΔE_d may be linked to such a structural change. The reason why hydrogen adsorption causes such a large structural change is discussed in detail in the ESI.

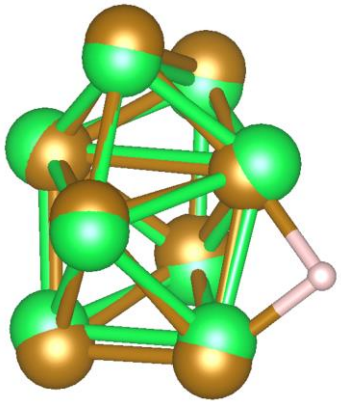

Fig. 9 Structural comparison of the Fe_8 nanocluster before and after hydrogen adsorption. The Fe atoms in the globally optimized structure with hydrogen adsorbed are shown in ochre, while those globally optimized without hydrogen are shown in green. The two are superimposed.

Hard as it might be to call ΔE_d as distortion energy in this study, the use of the distortion energy to analyze the energy by distinguishing between binding energy and adsorption energy may be novel in cluster science; we would like to add that such a way of analysis has been applied to a variety of energies, such as the activation energy of organic reactions [89, 90], the adsorption energy of a small molecule [91], the adhesion energy of a polymer [92].

3.4 Towards Catalyst Search

So far, we have systematically investigated the binding and adsorption energies of hydrogen to nanoclusters of different sizes of the three metals. The binding and adsorption energies were found to fall in the range of -3.4 to -2.1 eV and -3.4 to -1.4 eV, respectively. What is the best value for catalysis? However, it would be difficult to make a blanket statement. This is because the catalytic reactions that readers have in their minds vary from one person to the

next.

Here, we will limit our discussion to two important catalytic reactions involving hydrogen, namely the Haber-Bosch process and the Fischer-Tropsch process. In both, it is known that Ru works very well as a catalyst [83, 93]. The so-called B5 site on the stepped Ru (0001) surface is presumed to be an important active site in these catalytic reactions [94, 95, 96, 97, 98]. What the B5 site is all about is presented in Fig. 10a. Since cleavage of N-N and C-O bonds are important steps in these reactions [96, 98], the interaction of N, C, and O atoms with the surface might be worth investigating. Nevertheless, there is a paper by Tanaka and Tamaru [99], based on a large amount of data, that reported that regardless of the type of adsorbed atoms, the order of magnitude of the adsorption energy follows a common order determined by the type of metal. Thus, it may be possible to discuss the catalytic activity based only on the adsorption energy of hydrogen.

A simple slab model for the B5 site on a unique step-edge type model on Ru (0001) has been used by many theorists [97, 98, 100]. Referring to those previous studies, we created a model of the B5 site with one hydrogen atom adsorbed, as shown in Fig. 10a. Our slab model is composed of four Ru atomic layers of (3 × 4) supercell with two neighboring rows of Ru atoms in the top layer removed. A vacuum layer with a thickness of more than 12 Å was added on the surface. In the geometry optimization, the bottom two layers were held fixed at the bulk structure. The optimization was performed using VASP under the same conditions as those used

for the final optimization of the nanoclusters described in the Theoretical Methods section. However, there is one point of difference: k-point meshes with the reciprocal space resolution of $2\pi \times 0.05$ Å^{-1} were used here instead of the Γ-point sampling. For comparison, the adsorption of an H atom on the clean Ru (0001) surface was also calculated, where a slab model composed of four Ru atomic layers of (3 × 3) supercell was used. The result of this calculation can be interpreted as the adsorption of the H atom to a terrace site.

Figs 10a and 10b show the H adsorption structure at the B5 and terrace sites on the Ru (0001) surface. After calculating the various adsorption sites, it was found that the most stable adsorption mode is the bridge type at the B5 while the hollow at the terrace. For hydrogen adsorption on these surfaces, the binding and adsorption energies were evaluated as in the case of the metal nanoclusters. They are also shown in Fig. 10.

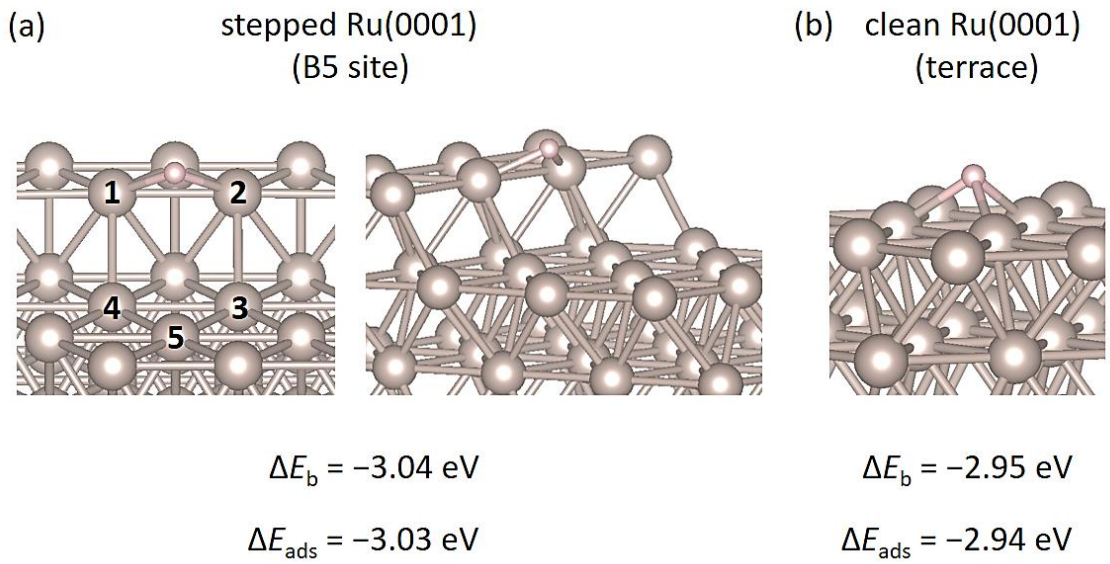

Fig. 10 (a) Structure of an H atom adsorbed at a B5 step-edge site on the Ru (0001) surface, seen from two different angles. 1-2-3-4-5 in the left panel indicates the B5. (b) That at a hollow site on the clean Ru (0001) surface (terrace). Below each structure, the values of ΔE_b and ΔE_{ads} calculated for the H adsorption are shown.

The difference between ΔE_b and ΔE_{ads} for these surfaces is very small, about 0.01 eV, highlighting the difference from the metal nanoclusters. This suggests that there is little need to discuss these energies separately for the solid metal surfaces. Comparing the values of ΔE_b and ΔE_{ads} for the H atom adsorption at the B5 and terrace sites, their absolute values for the B5 site are larger than those for the terrace by about 0.1 eV, suggesting that the B5 is more active for hydrogen adsorption. This is probably due to the highly coordinatively unsaturated nature of the Ru atoms at the step edge. Such a difference was also observed in the adsorption of other atoms and molecules to the Ru surfaces in a preceding theoretical calculation [96].

Keeping in mind the binding and adsorption energies of hydrogen at the B5 site on the Ru surface, when looking at Figs 5 and 6, Fe_5 catches the eye: both ΔE_b and ΔE_{ads} for Fe_5 are

about -3.0 eV. Also, the distortion energy for Fe_5 is very small, so we have a feeling that Fe_5 will work as a robust catalyst. One thing to keep in mind when interpreting these energies is that the actual catalyst surface will not be as clean as the ones shown in Figs 2, 3, and 10. If it is allowed to assume that the degree of change in the adsorption energy due to the co-adsorption of other molecules is equal between the Ru surface and the cluster surface, then the above reasoning would be correct. In any case, this is an issue to be examined in the future. We are working on theoretical studies of catalytic reactions using Fe_5.

We have not yet reached the goal of this study that we are aiming for. We still have a long way to go. However, we have prepared this manuscript with the feeling that we have reached a milestone. In closing, we would like to discuss the issues that need to be addressed in the future. In this study, we explored the cluster structure with only one hydrogen atom adsorbed. However, it may not be true that only one hydrogen atom will be adsorbed in the actual catalytic process. How the stable structure and adsorption energy change as the number of adsorbed hydrogen atoms increases is an issue that remains to be investigated. Of course, as the number of atoms in the system increases, the computational cost increases exponentially.

Most of the industrially relevant metal nanoparticle catalysts are much larger than the nanoclusters we have studied in this work [101], and it would be difficult to approach them with the current computational resources. On the other hand, in recent years, it has become possible to synthesize clusters of similar size to those studied in this research [102], and the

method presented here can be applied to catalysis using such clusters.

In this study, we have been obsessed with the search for the most stable cluster structure. However, recent studies on cluster catalysts have interestingly shown that metastable rather than global minimum structures may govern the kinetics of the catalysis [103]. By using the local PSO algorithm [104], one may be able to effectively obtain not only global minimum structures but also metastable structures, which may be beneficial for pursuing such a challenge.

4 Conclusion

For Fe, Ni, and Cu, which are frequently used as catalysts, we have explored stable nanocluster structures. This was effectively done by using the particle swarm optimization algorithm. A systematic and comprehensive structural search was conducted, starting with the number of atoms of 1 and ending up to 10. The same method was also used to search for those with a single hydrogen atom adsorbed. Using the nanocluster structure obtained from the structure search, we analyzed the interaction between hydrogen and the clusters. As a result, we found that the strength of the interaction depends on the metal species and cluster size. It was found that the dependence of the interaction strength on the cluster size is small for Ni, but for Fe and Cu, it varies greatly with the cluster size. It was often observed for Cu that the stable structure differs between the hydrogen-adsorbed state and the metal-only state. This may reflect the softness of the Cu clusters. When taking into account the robustness as a catalyst, we might

exclude Cu as an option.

Finally, based on our estimate of the affinity of a hydrogen atom to the active site of a typical catalyst, Ru, we predicted that an interaction energy of ca. -3 eV for hydrogen would be suitable for catalysis. A metal nanocluster that satisfies this requirement is Fe_5, which appears to be a robust catalyst with very little structural change upon hydrogen adsorption. Although our research is still in its infancy, we believe that this manuscript contains some useful information, and hence we would like to present it as a suggestion for one of the possible methodologies of catalyst discovery.

Supplementary Information The online version contains supplementary material available at https://doi.org/XXX

Acknowledgements

The computation in this work was primarily performed using the ITO supercomputer system at the Research Institute for Information Technology of Kyushu University. This work was financially supported by KAKENHI grants (numbers JP17K14440, JP17H03117, and JP21K04996) from the Japan Society for the Promotion of Science (JSPS) and the Ministry of Education, Culture, Sports, Science and Technology of Japan (MEXT) through the MEXT projects Integrated Research Consortium on Chemical Sciences, Cooperative Research Program of Network Joint Research Center for Materials and Devices and Elements Strategy Initiative to Form Core Research Center, and by JST-CREST JPMJCR15P5 and JST-Mirai JPMJMI18A2. Y.T. is especially grateful for a JSPS Grant-in-Aid for Scientific Research on Innovative Areas (Discrete Geometric Analysis for Materials Design, grant number

JP20H04643, and Mixed Anion, grant number JP19H04700).

Conflict of interest

The authors do not have conflicts of interest to declare.

References

1. Álvarez-Collado JR (2006) On the theoretical description of the chemisorption of the hydrogen atom on the metallic surface. Calculation of energy interaction of H with hcp Co and Ni surface clusters. Surf Sci 600:133-142

2. Ertl G (2008) Reactions at surfaces: from atoms to complexity. Angew Chem Int Ed 47:3524-3535

3. de Smit E, Weckhuysen BM (2008) The renaissance of iron-based Fischer-Tropsch synthesis: on the multifaceted catalyst deactivation behavior. Chem Soc Rev 37:2758-2781

4. Thüne PC, Weststrate CJ, Moodley P, Saib AM, van de Loosdrecht J, Miller JT, Niemantsverdriet JW (2011) Studying Fischer-Tropsch catalysts using transmission electron microscopy and model systems of nanoparticles on planar supports. Catal Sci Technol 1:689-697

5. Gao R, Liu X, Cao Z, Liu X, Lu K, Ma D, Yang Y, Li Y, Hoffmann R, Wen X (2019) Carbon permeation: the prerequisite elementary step in iron-catalyzed Fischer-Tropsch synthesis. Catal Lett 149:645-664

6. Wang T, Wang S, Luo Q, Li Y, Wang J, Beller M, Jiao H (2014) Hydrogen adsorption structures and energetics on iron surfaces at high coverage. J Phys Chem C 118:4181-4188

7. Che M (2013) Nobel prize in chemistry 1912 to Sabatier: organic chemistry or catalysis? Catal Today 218-219:162-171

8. Wang W, Wang S, Ma X, Gong J (2011) Recent advances in catalytic hydrogenation of carbon dioxide. Chem Soc Rev 40:3703-3727

9. Walker DM, Pettit SL, Wolan JT, Kuhn JN (2012) Synthesis gas production to desired hydrogen to carbon monoxide ratios by tri-reforming of methane using Ni–MgO–(Ce,Zr)O_2 catalysts. Appl Catal A 445-446:61-68

10. Wang W, Zhao Y (2014) Dissociation rates of H_2 on a Ni(100) surface: the role of the physisorbed state. Phys Chem Chem Phys 16:13318-13328

11. Zhao H, He Y, Zhao Y, Wang W (2018) H_2 dissociation on H precovered Ni(111) surfaces: coverage dependence, lattice motion, and arrangement effects. J Phys Chem C 122:574-583

12. Saillard JY, Hoffmann R (1984) Carbon-hydrogen and hydrogen-hydrogen activation in transition metal complexes and on surfaces. J Am Chem Soc 106:2006-2026

13. Yong ST, Ooi CW, Chai SP, Wu XS (2013) Review of methanol reforming-Cu-based catalysts, surface reaction mechanisms, and reaction schemes. Int J Hydrog Energy 38:9541-9552.

14. Gharda KH, Sliepcevich CM (1960) Copper catalysts in hydrogenating nitro-benzene to aniline. Ind Eng Chem 52:417-420

15. Rioux RM, Vannice MA Hydrogenation/dehydrogenation reactions: isopropanol dehydrogenation over copper catalysts. J Catal 216:362-376

16. Zaccheria F, Ravasio N, Psaro R, Fusi A (2006) Synthetic scope of alcohol transfer dehydrogenation catalyzed by Cu/Al_2O_3: a new metallic catalyst with unusual selectivity. Chem Eur J 12:6426-6431

17. Álvarez-Falcón L, Viñes F, Notario-Estévez A, Illas F (2016) On the hydrogen adsorption and dissociation on Cu surfaces and nanorows. Surf Sci 646:221-229

18. Bonfanti M, Diaz C, Somers MF, Kroes GJ (2011) Hydrogen dissociation on Cu(111): the influence of lattice motion. Part I. Phys Chem Chem Phys 13:4552-4561

19. Liu L, Corma A (2018) Metal catalysts for heterogeneous catalysis: from single atoms to nanoclusters and nanoparticles. Chem Rev 118:4981-5079

20. Fernández E, Boronat M (2019) Sub nanometer clusters in catalysis. J Phys Condens Matter 31:013002

21. Negreiros FR, Halder A, Yin C, Singh A, Barcaro G, Sementa L, Tyo EC, Pellin MJ, Bartling S, Meiwes-Broer K-H, Seifert S, Sen P, Nigam S, Majumder C, Fukui N, Yasumatsu H, Vajda S, Fortunelli A (2018) Bimetallic Ag-Pt sub-nanometer supported clusters as highly efficient and robust oxidation catalysts. Angew Chem Int Ed 57:1209-1213

22. Choi H, Oh S, Park JY (2020) High methane selective Pt cluster catalyst supported on Ga_2O_3 for CO_2 hydrogenation. Catal Today 352:212-219

23. Eberhardt W (2002) Clusters as new materials. Surf Sci 500:242-270

24. Kitano M, Kanbara S, Inoue Y, Kuganathan N, Sushko PV, Yokoyama T, Hara M, Hosono H (2015) Electride support boosts nitrogen dissociation over ruthenium catalyst and shifts the bottleneck in ammonia synthesis. Nat Commun 6:6731

25. Tada S, Otsuka F, Fujiwara K, Moularas C, Deligiannakis Y, Kinoshita Y, Uchida S, Honma T, Nishijima M, Kikuchi R (2020) Development of CO_2-to-methanol hydrogenation catalyst by focusing on the coordination structure of the Cu species in spinel-type oxide $Mg_{1-x}Cu_xAl_2O_4$. ACS Catal 10:15186-15194

26. Mu X-D, Meng J-Q, Li Z-C, Kou Y (2005) Rhodium nanoparticles stabilized by ionic

copolymers in ionic liquids: long lifetime nanocluster catalysts for benzene hydrogenation. J Am Chem Soc 127:9694-9695

27. Kon K, Siddiki SMAH, Shimizu K (2013) Size- and support-dependent Pt nanocluster catalysis for oxidant-free dehydrogenation of alcohols. J Catal 304:63-71

28. Zhu L, Liang Y, Sun L, Wang J, Xu D (2021) Highly efficient dehydrogenation of formic acid over binary palladium–phosphorous alloy nanoclusters on N-doped carbon. Inorg Chem 60:10707-10714

29. Singha RK, Tsuji Y, Mahyuddin MH, Yoshizawa K (2019) Methane activation at the metal–support interface of Ni_4-CeO_2(111) catalyst: a theoretical study. J Phys Chem C 123:9788-9798

30. Cheng Z, Lo C (2013) Effect of support structure and composition on the catalytic activity of Pt nanoclusters for methane dehydrogenation. Ind Eng Chem Res 52:15447-15454

31. Abdollahi T, Farmanzadeh D (2018) Graphene-supported Cu_{11} nanocluster as a candidate catalyst for the selective hydrogenation of acetylene: a density functional study. J Alloys Compd 735:117-130

32. Latimer AA, Kulkarni AR, Aljama H, Montoya JH, Yoo JS, Tsai C, Abild-Pedersen F, Studt F, Nørskov JK (2017) Understanding trends in C-H bond activation in heterogeneous catalysis. Nat Mater 16:225-229

33. Liu C, Li G, Pidko EA Property-activity relations for methane activation by dual-metal Cu–oxo trimers in ZSM-5 zeolite. Small Methods 2:1800266

34. Kobayashi Y, Tang Y, Kageyama T, Yamashita H, Masuda N, Hosokawa S, Kageyama H (2017) Titanium-based hydrides as heterogeneous catalysts for ammonia synthesis. J Am Chem Soc 139:18240-18246

35. Cao Y, Saito A, Kobayashi Y, Ubukata H, Tang Y, Kageyama H (2021) Vanadium hydride as an ammonia synthesis catalyst. ChemCatChem 13:191-195

36. Tsuji Y, Okazawa K, Kobayashi Y, Kageyama H, Yoshizawa K (2021) Electronic origin of catalytic activity of TiH_2 for ammonia synthesis. J Phys Chem C 125:3948-3960

37. Wu J, Ong SW, Kang HC, Tok ES (2010) Hydrogen adsorption on mixed platinum and nickel nanoclusters: the influence of cluster composition and graphene support. J Phys Chem C 114:21252-21261

38. Kirsankin AA, Dohlikova NV, Sarvadii SY (2018) The study of adsorption of hydrogen onto copper and gold clusters by method of the density functional. IOP Conf Ser Mater Sci Eng 347:012018.

39. Takahashi K, Isobe S, Omori K, Mashoff T, Convertino D, Miseikis V, Coletti C, Tozzini V, Heun S (2016) Revealing the multibonding state between hydrogen and graphene-supported Ti clusters. J Phys Chem C 120:12974-12979

40. Takahashi K, Isobe S (2014) Enhancing the hydrogen storage capacity of TiFe by utilizing clusters. Phys Chem Chem Phys 16:16765-16770

41. Takahashi K, Isobe S, Ohnuki S (2013) Chemisorption of hydrogen on Fe clusters through hybrid bonding mechanisms. Appl Phys Lett 102:113108

42. Blum C, Li X (2008) Swarm intelligence in optimization. In: Blum C, Merkel D (eds) Swarm intelligence introduction and applications. Springer, Berlin, pp 43-85

43. Watson GW, Wells RPK, Willock DJ, Hutchings GJ (2000) Ab initio simulation of the interaction of hydrogen with the {111} surfaces of platinum, palladium and nickel. A possible explanation for their difference in hydrogenation activity. Chem Commun 705-706

44. Michaelian K, Rendon N, Garzon IL (1999) Structure and energetics of Ni, Ag, and Au nanoclusters. Phys Rev B 60:2000-2010

45. Matus MF, Malola S, Kinder Bonilla E, Barngrover B, Aikens CM, Häkkinen H (2020) A topological isomer of the $Au_{25}(SR)_{18}^{-}$ nanocluster. Chem Commun 56:8087-8090

46. Tanaka H, Neukermans S, Janssens E, Silverans RE, Lievens P (2003) Density functional study on structure and stability of bimetallic Au_NZn ($N \leqslant 6$) clusters and their cations. J Chem Phys 119:7115-7123

47. Tanaka H, Neukermans S, Janssens E, Silverans RE, Lievens P (2003) J Am Chem Soc 125:2862-2863

48. Wang Y, Lv J, Zhu L, Ma Y (2010) Crystal structure prediction via particle-swarm optimization. Phys Rev B 82:094116

49. Wang Y, Lv J, Zhu L, Ma Y (2012) CALYPSO: a method for crystal structure prediction. Comput Phys Commun 183:2063-2070

50. Gao B, Gao P, Lu S, Lv J, Wang Y, Ma Y (2019) Interface structure prediction via CALYPSO method. Sci Bull 64:301-309

51. Kennedy J, Eberhart RC (1997) A discrete binary version of the particle swarm algorithm. In: 1997 IEEE international conference on systems, man, and cybernetics. Computational cybernetics and simulation, vol 5, pp 4104-4108

52. Eberhart RC, Shi YH (2001) Particle swarm optimization: developments, applications and resources. In: Proceedings of the 2001 congress on evolutionary computation, Seoul, South Korea, vol 1, pp 81-86

53. Yamashita T, Sato N, Kino H, Miyake T, Tsuda K, Oguchi T (2018) Crystal structure prediction accelerated by Bayesian optimization. Phys Rev Materials 2:013803

54. Hodgson R J W (2002) Particle swarm optimization applied to the atomic cluster optimization problem. In: Proc. of Genetic and Evolut. Comput. Conf., pp. 68–73.

55. Call ST, Zubarev DY, Boldyrev AI (2007) Global minimum structure searches via particle

swarm optimization. J Comput Chem 28:1177–1186

56. Kresse G, Furthmüller J (1996) Efficient iterative schemes for ab initio total-energy calculations using a plane-wave basis set. Phys Rev B 54:11169-11186

57. Kresse G, Hafner J (1993) Ab initio molecular dynamics for liquid metals. Phys Rev B 47:558-561

58. Kresse G, Hafner J (1994) Ab initio molecular-dynamics simulation of the liquid-metal-amorphous-semiconductor transition in germanium. Phys Rev B 49:14251-14269

59. Kresse G, Furthmüller J (1996) Efficiency of ab-initio total energy calculations for metals and semiconductors using a plane-wave basis set. Comput Mater Sci 6:15-50

60. Hori M, Tsuji Y, Yoshizawa K (2021) Bonding of C_1 fragments on metal nanoclusters: a search for methane conversion catalysts with swarm intelligence. Phys Chem Chem Phys 23: 14004-14015

61. Tsuji Y, Hoffmann R, Miller JS (2016) Revisiting $Ir(CO)_3Cl$. Polyhedron 103:141-149

62. Lv P, Lu Z, Li S, Ma D, Zhang W, Zhang Y, Yang Z (2016) Tuning metal cluster catalytic activity with morphology and composition: a DFT study of O_2 dissociation at the global minimum of Pt_mPd_n (m + n = 5) clusters. RSC Adv 6:104388-104397

63. Jin Y, Lu S, Hermann A, Kuang X, Zhang C, Lu C, Xu H, Zheng W (2016) Probing the structural evolution of ruthenium doped germanium clusters: photoelectron spectroscopy and density functional theory calculations. Sci Rep 6:30116

64. Li CG, Yuan YQ, Hu YF, Zhang J, Tang YN, Ren BZ (2016) Density functional theory study of the structures and electronic properties of copper and sulfur doped copper clusters. Comput Theor Chem 1080:47–55

65. Qin W, Lu W-C, Xia L-H, Zhao L-Z, Zang Q-J, Wang CZ, Ho KM (2015) Structures and stability of metal-doped Ge_nM (n = 9, 10) clusters. AIP Adv 5:067159

66. Tsuji Y, Yoshizawa K (2021) From infection clusters to metal clusters: significance of the lowest occupied molecular orbital (LOMO). ACS Omega 6:1339-1351.

67. Rogan J, Ramírez M, Mu noz V, Valdivia J, García G, Ramírez R, Kiwi M (2009) Diversity driven unbiased search of minimum energy cluster configurations. J Phys Condens Matter 21:084209

68. Takahashi K, Takahashi L, Miyazato I, Fujima J, Tanaka Y, Uno T, Satoh H, Ohno K, Nishida M, Hirai K (2019) The rise of catalyst informatics: towards catalyst genomics. ChemCatChem 11:1146-1152

69. Nguyen TN, Nhat TTP, Takimoto K, Thakur A, Nishimura S, Ohyama J, Miyazato I, Takahashi L, Fujima J, Takahashi K, Taniike T (2020) High-throughput experimentation and catalyst informatics for oxidative coupling of methane. ACS Catal 10:921-932

70. Kamachi T, Saito M, Tsuji Y, Yoshizawa K (2017) Catalyst informatics on methane activation on various metal alloys. J Comput Chem Jpn 16:147-148

71. Perdew JP, Burke K, Ernzerhof M (1996) Generalized gradient approximation made simple. Phys Rev Lett 77:3865-3868

72. Blöchl PE (1994) Projector augmented-wave method. Phys Rev B 50:17953-17979

73. Kresse G, Joubert D (1999) From ultrasoft pseudopotentials to the projector augmented-wave method. Phys Rev B 59:1758-1775

74. Grimme S. (2006) Semiempirical GGA-type density functional constructed with a long-range dispersion correction. J Comput Chem 27:1787-1799

75. Momma K, Izumi F (2011) VESTA 3 for three-dimensional visualization of crystal, volumetric and morphology data. J Appl Crystallogr 44:1272-1276

76. Cheung PM, Berger RF, Zakharov LN, Gilbertson JD (2016) Square planar Cu (I) stabilized by a pyridinediimine ligand. Chem Commun 52:4156-4159

77. Hanss J, Kruger HJ (1996) The first stable copper(III) complex containing aliphatic thiolates as ligands: structural and spectroscopic evidence for Cu^{II} and Cu^{III} ions in complexes with square-planar CuN_2S_2 coordination environments. Angew Chem Int Ed 35:2827-2830

78. Gustafsson B, Håkansson M, Jagner S (2003) Copper (II) is harder than copper (I): a novel mixed-valence example from alkoxide chemistry. New J Chem 27:459-461

79. Albright TA, Burdett JK, Whangbo MH (1985) Orbital interactions in chemistry. Wiley, New York

80. Tsuji Y, Dasari PLVK, Elatresh SF, Hoffmann R, Ashcroft NW Structural diversity and electron confinement in Li_4N: potential for 0-D, 2-D, and 3-D electrides. J Am Chem Soc 138:14108-14120

81. It would also be interesting that the peaks almost completely overlap for the case of Ni; however, we have confirmed that the peak height is lowered when the RDF is calculated using only the n = 9 and 10 cluster structures.

82. Tyo EC, Yin CR, Di Vece M, Qian Q, Kwon G, Lee S, Lee B, DeBartolo JE, Seifert S, Winans RE, Si R, Ricks B, Goergen S, Rutter M, Zugic B, Flytzani-Stephanopoulos M, Wang ZW, Palmer RE, Neurock M, Vajda S (2012) Oxidative dehydrogenation of cyclohexane on cobalt oxide (Co_3O_4) nanoparticles: the effect of particle size on activity and selectivity. ACS Catal 2:2409-2423

83. Aika K, Ozaki A, Hori H (1972) Activation of nitrogen by alkali metal promoted transition metal I. Ammonia synthesis over ruthenium promoted by alkali metal. J Catal 27:424-431

84. Siporin SE, Davis RJ (2004) Use of kinetic models to explore the role of base promoters on Ru/MgO ammonia synthesis catalysts. J Catal 225:359-368

85. Kitano M, Inoue Y, Ishikawa H, Yamagata K, Nakao T, Tada T, Matsuishi S, Yokoyama T, Hara M, Hosono H (2016) Essential role of hydride ion in ruthenium-based ammonia synthesis catalysts. Chem Sci 7:4036-4043

86. Toyoshima I, Somorjai GA (1979) Heats of chemisorption of O_2, H_2, CO_2, and N_2 on polycrystalline and single crystal transition metal surfaces. Catal Rev 19:105-159

87. The H atom weakens the metal-metal bond and increases the length.

88. The spin state with a magnetic moment of 24 μ_B was identified as the most stable state for both Fe_8 clusters.

89. Ess DH, Houk KN (2007) Distortion/interaction energy control of 1,3-dipolar cycloaddition reactivity. J Am Chem Soc 129:10646-10647

90. Bickelhaupt FM (1999) Understanding reactivity with Kohn-Sham molecular orbital theory: E2-S_N2 mechanistic spectrum and other concepts. J Comput Chem 20:114-128

91. Tsuji Y, Yoshizawa K (2018) Adsorption and activation of methane on the (110) surface of rutile-type metal dioxides. J Phys Chem C 122:15359-15381

92. Higuchi C, Tanaka H, Yoshizawa K (2019) Molecular understanding of the adhesive interactions between silica surface and epoxy resin: effects of interfacial water. J Comput Chem 40:164-171

93. van Der Laan GP, Beenackers AACM (1999) Kinetics and selectivity of the Fischer-Tropsch synthesis: a literature review. Catal Rev Sci Eng 41:255-318

94. van Hardeveld R, van Montfoort A (1966) The influence of crystallite size on the adsorption of molecular nitrogen on nickel, palladium and platinum. Surf Sci 4:396-430

95. Jacobsen CJH, Dahl S, Hansen PL, Tornqvist E, Jensen L, Topsoe H, Prip DV, Moenshaug PB, Chorkendorff I (2000) Structure sensitivity of supported ruthenium catalysts for ammonia synthesis. J Mol Catal A: Chem 163:19-26

96. Logadóttir Á, Nørskov JK (2003) Ammonia synthesis over a Ru(0001) surface studied by density functional calculations. J Catal 220:273-279

97. Liu Z-P, Hu P (2002) A new insight into Fischer-Tropsch synthesis. J Am Chem Soc 124:11568-11569

98. Li HP, Fu G, Xu X (2012) A new insight into the initial step in the Fischer-Tropsch synthesis: CO dissociation on Ru surfaces. Phys Chem Chem Phys 14:16686-16694

99. Tanaka K, Tamaru K (1963) A general rule in chemisorption of gases on metals. J Catal 2:366-370

100. Arevalo RL, Aspera SM, Escano MCS, Nakanishi H, Kasai H (2017) First principles study of methane decomposition on B5 step-edge type site of Ru surface. J Phys: Condens Matter 29:184001

101. Kleis J, Greeley J, Romero NA, Morozov VA, Falsig H, Larsen AH, Lu J, Mortensen JJ, Dulak M, Thygesen KS, Norskov JK, Jacobsen KW (2011) Finite size effects in chemical bonding: From small clusters to solids. Catal Lett 141:1067–1071

102. Tsukamoto T, Kambe T, Imaoka T, Yamamoto K (2021) Modern cluster design based on experiment and theory. Nat Chem Rev 5:338– 347

103. Zhang Z, Zandkarimi B, Alexandrova AN (2020) Ensembles of metastable states govern heterogeneous catalysis on dynamic interfaces. Acc Chem Res 53:447–458

104. Wang H, Wang Y, Lv J et al (2016) CALYPSO structure prediction method and its wide application. Comput Mater Sci 112:406–415